TO THE EDITOR:

RBCs prevent rapid PIEZO1 inactivation and expose slow deactivation as a mechanism of dehydrated hereditary stomatocytosis

Elizabeth L. Evans,[1,*] Oleksandr V. Povstyan,[1,*] Dario De Vecchis,[1] Fraser Macrae,[1] Laeticia Lichtenstein,[1] T. Simon Futers,[1] Gregory Parsonage,[1] Neil E. Humphreys,[2] Antony Adamson,[2] Antreas C. Kalli,[1] Melanie J. Ludlow,[1] and David J. Beech[1]

[1]School of Medicine, University of Leeds, Leeds, United Kingdom; and [2]Faculty of Biology, Medicine and Health, University of Manchester, AV Hill Building, Manchester, United Kingdom

The discovery of PIEZO proteins has enabled better understanding of how cells respond to mechanical force.[1-3] PIEZOs assemble to form ion channels that link force to cell behavior via transmembrane cation flux.[1,2,4] Shortly after the initial PIEZO discoveries, associations of *PIEZO1* mutations with xerocytosis/dehydrated hereditary stomatocytosis (DHS)[4-15] and links to malarial resistance were suggested.[16] PIEZO1 channels are now an established feature of red blood cell (RBC) biology where they regulate intracellular Ca^{2+} and cell hydration in coordination with other mechanisms such as the Gardos channel.[17-20] However, studies of PIEZO1 reconstituted in cell lines have suggested that the channels activate within milliseconds and then inactivate (desensitize) completely within a few hundred milliseconds when rapidly stimulated by increases in membrane tension caused by pulling on the membrane or cell deformation via a probe.[1,4,7,9,18] DHS mutations have been found to slow the fast inactivation process, which represents gain of function.[7-9,18] It is, however, unclear how such rapid events are relevant to RBC physiology. Moreover, although the available data are limited because of the low prevalence of DHS, studies of RBCs from patients suggest sustained channel activity unlike that reported for PIEZO1 in cell lines.[6,10,12,15] Therefore, we sought additional understanding through electrophysiological analysis of murine RBCs. To mechanically stimulate the channels, we applied shear stress, a frictional force created physiologically by blood flow. To understand the impact of DHS mutation, we generated the murine equivalent of one of the first-identified DHS mutations, M2225R.[4,5,8,9]

In mouse PIEZO1, the equivalent of M2225R is M2241R. Molecular modeling and pharmacological analysis of overexpressed channels suggested suitability of mouse PIEZO1 as a model for human PIEZO1 (supplemental Results; supplemental Figures 1 and 2, available on the *Blood* Web site). Furthermore, 8-week-old mice homozygous for M2241R ($PIEZO1^{M\text{-}R/M\text{-}R}$; supplemental Results; supplemental Figures 3 and 4) displayed features consistent with DHS that included stomatocytosis (supplemental Figure 5); decreased osmotic fragility (supplemental Figure 6); decreased hemoglobin, hematocrit, and RBC count (supplemental Table 1); and increased RBC and hemoglobin concentration distribution widths and percentage of reticulocytes (supplemental Table 1). There were no significant changes in spleen weight (supplemental Figure 7) or liver function test results (supplemental Table 2). There were potential changes in plasma iron and total iron binding capacity that did not reach statistical significance, but transferrin showed a small significant increase (supplemental Table 2). $PIEZO1^{M\text{-}R/M\text{-}R}$ mice were born at slightly lower frequency than wild-type (WT) mice, suggesting a potential deleterious effect, but the adult $PIEZO1^{M\text{-}R/M\text{-}R}$ mice appeared normal, and body weight gain was not different from that in WT mice (supplemental Figure 8). However, increased spleen weight in the $PIEZO1^{M\text{-}R/M\text{-}R}$ mice at 22 weeks of age suggests the potential for age-related changes in phenotype (supplemental Figure 7). All remaining experiments focused on mice at 8 weeks of age. Heterozygous mice ($PIEZO1^{WT/M\text{-}R}$) showed a decrease in osmotic fragility, but less than for the $PIEZO1^{M\text{-}R/M\text{-}R}$ mice, which suggests an intermediate phenotype (supplemental Figure 6). The $PIEZO1^{WT/M\text{-}R}$ mice were born at the expected Mendelian ratio (supplemental Figure 8).

To understand the effect of M2241R on channel properties, patch-clamp electrophysiology was applied to RBCs freshly isolated from mice. For physiological relevance, we first used the perforated-patch whole-cell configuration to achieve membrane potential measurements. Resting membrane potential data are provided in the supplemental Information. For most experiments, constant current was injected to hyperpolarize RBCs to −80 mV and thereby maximize visibility of PIEZO1-related responses to fluid flow of 20 $\mu L \cdot s^{-1}$, a rate that occurs in mice.[21] There was a small depolarization in response to the fluid flow in WT RBCs, consistent with the opening of PIEZO1 channels (Figure 1A; mean data in Figure 1D). The depolarization was sustained for at least 20 seconds. After flow ceased, the membrane potential returned to its initial value (Figure 1A,D). Depolarization tended to be larger in $PIEZO1^{WT/M\text{-}R}$ and was larger ($P < .05$) in $PIEZO1^{M\text{-}R/M\text{-}R}$ RBCs, but the most striking difference was failure to recover after flow ceased (Figure 1B-C; mean data in Figure 1D). To further investigate, we switched to voltage-clamp mode. In WT RBCs, fluid flow caused inward current as expected, which then decayed slowly after about 10 seconds (Figure 1F; mean data in Figure 1I). In $PIEZO1^{WT/M\text{-}R}$ and $PIEZO1^{M\text{-}R/M\text{-}R}$ RBCs, the initial response was similar to that in WT, except the slow inactivation was mostly absent (Figure 1G,H). Most striking, there was failure of current to recover after cessation of fluid flow (Figure 1G-H; mean data in Figure 1I). GsMTx4, an inhibitor of PIEZO1 channel activity,[22] abolished all depolarizing and inward current activities (Figure 1E,J; supplemental Figures 9 and 10). An intriguing finding was that washout of GsMTx4 from mutant RBCs revealed recovery to activity that was more like the activity of WT RBCs than that of mutant RBCs in the absence of toxin, suggesting the potential to correct mutant channel behavior (supplemental Figures 9 and 10).

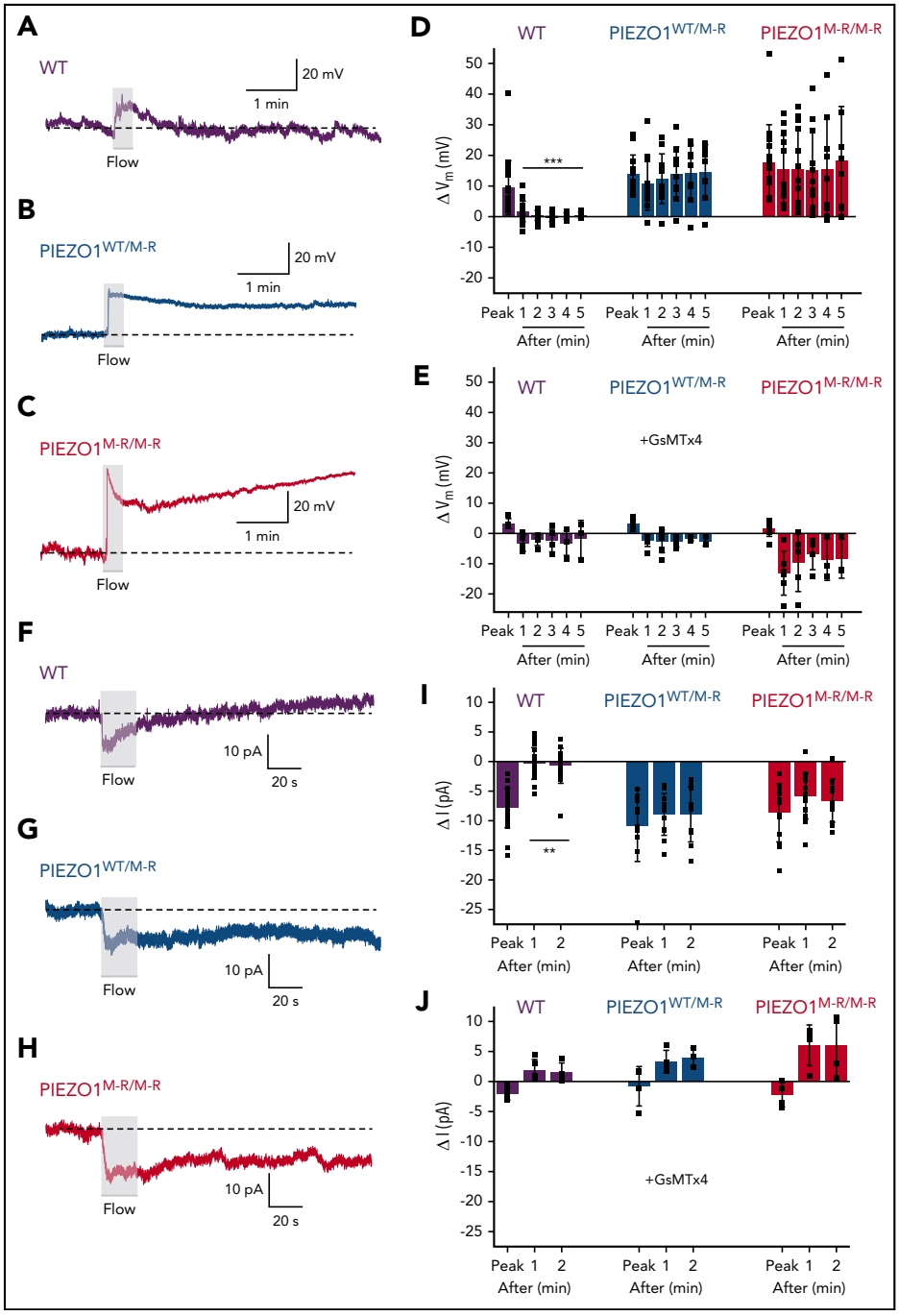

Figure 1. Slow kinetics of RBC PIEZO1 mice and slow recovery in PIEZO1$^{WT/M-R}$ and PIEZO1$^{M-R/M-R}$ mice. (A-C) Membrane potential (V_m) recordings obtained using the perforated-patch, whole-cell mode applied to freshly isolated RBCs from WT (A), PIEZO1$^{WT/M-R}$ (B), and PIEZO1$^{M-R/M-R}$ (C) mice. RBCs were exposed to 20 μL·s^{-1} fluid flow for 20 seconds, as indicated by the shaded areas. (D) Summary data for experiments of the type shown in panels A-C. Presented is the peak (maximum [max]) change in V_m of WT, PIEZO1$^{WT/M-R}$, and PIEZO1$^{M-R/M-R}$ RBC counts after exposure to flow and V_m at 1 to 5 minutes after flow. Averaged data are displayed as means ± standard deviation, and each data point is shown. WT: n = 20 (max, 1 minute), 16 (2 minutes), 13 (3 minutes), and 9 (4 and 5 minutes); PIEZO1$^{WT/M-R}$: n = 13 (max), 12 (1 minute), 11 (2 minutes), 10 (3 minutes), and 9 (4 and 5 minutes); and PIEZO1$^{M-R/M-R}$: n = 14 (max, 1 minute), 13 (2 minutes), 11 (3 minutes), 9 (4 minutes), and 8 (5 minutes). (E) As in panel D, except with 2.5 μM GsMTx4 in the extracellular solution. WT: n = 5 (max, 1 minute, 2 minutes, 3 minutes), 4 (4 minutes), and 3 (5 minutes); PIEZO1$^{WT/M-R}$: n = 7 (max, 1 minute), 6 (2 minutes), 4 (3 and 4 minutes), 3 (5 minutes); and PIEZO1$^{M-R/M-R}$: n = 8 (max), 6 (1 minute), 5 (2 minutes), 4 (3 minutes), and 3 (4 and 5 minutes). (F-H) Ionic current recordings obtained using the perforated-patch technique in whole-cell, voltage-clamp mode applied to freshly isolated RBCs from WT (F), PIEZO1$^{WT/M-R}$ (G), and PIEZO1$^{M-R/M-R}$ mice (H). RBCs were exposed to 20 μL·s^{-1} fluid flow for 20 seconds, as indicated by the shaded areas. Holding voltage was −80 mV. (I) Summary data for experiments of the type shown in panels F-H. Presented is the peak (max) change in current (ΔI) of WT, PIEZO1$^{WT/M-R}$ RBCs after exposure to flow and then the ΔI at 1 and 2 minutes after flow. Averaged data are means ± standard deviation, and individual data points are shown. WT: n = 23 (max, 1 minute) and 15 (2 minutes); PIEZO1$^{WT/M-R}$: n = 12 (max, 1 minute) and 10 (2 minutes); and PIEZO1$^{M-R/M-R}$: n = 18 (max), 15 (1 minute), and 11 (2 minutes). (J) As in panel I, except with 2.5 μM GsMTx4 in the extracellular solution. WT: n = 5 (max, 1 minute, 2 minutes); PIEZO1$^{WT/M-R}$: n = 4 (max, 1 minute), 3 (2 minutes); and PIEZO1$^{M-R/M-R}$: n = 4 (max, 1 minute, 2 minutes). Statistical analysis by one-way ANOVA with Bonferroni's post hoc test indicated: (D,I) significant decay of the WT (**$P < .01$; *** $P < .001$) but not mutant RBC responses; (D) significant increase in the peak response in PIEZO1$^{M-R/M-R}$ RBCs compared with WT ($P < .05$); (E) no significant effects of flow in WT or PIEZO1$^{WT/M-R}$, but significant hyperpolarization at 1 minute compared with the peak in PIEZO1$^{M-R/M-R}$ ($P < .01$); and (J) no significant effects of flow in WT or PIEZO1$^{WT/M-R}$ but significant outward current at 1 and 2 minutes compared with peak in PIEZO1$^{M-R/M-R}$ ($P < .001$).

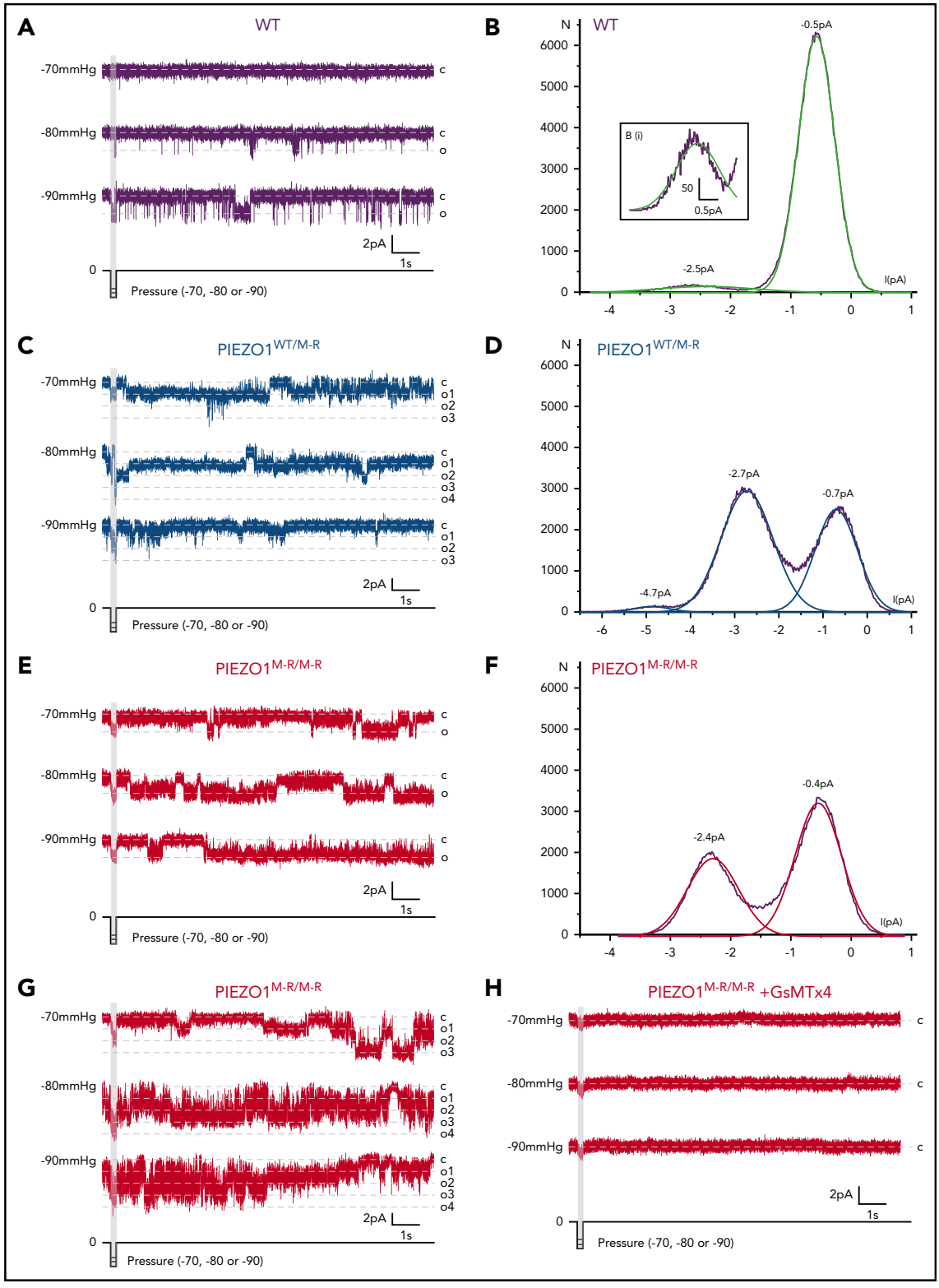

Figure 2. Failure of deactivation in PIEZO1$^{WT/M-R}$ and PIEZO1$^{M-R/M-R}$ single channels. Data are for single-channel activity measured by the cell-attached patch technique applied to freshly isolated RBCs of WT (A-B), PIEZO1$^{WT/M-R}$ (C-D), and PIEZO1$^{M-R/M-R}$ (E-H) mice. A fast pressure-clamp system applied brief (200 ms) negative pressure pulses to the patches, as indicated below the original exemplar current traces (A,C,E,G,H). Dashed horizontal lines indicate current levels for closed channels (c) and open channels (o, or o1-4 for multiple channel openings in panels C and G). Constant voltage of +80 mV was applied to the patch pipette. (A,E) Data are considered to be for patches each containing only 1 PIEZO1 channel; (C,G) patches contain multiple PIEZO1 channels. (B,D,F) Amplitude histogram analysis for the exemplar traces, showing plots of the frequency of detection of events (N) at the current amplitudes indicated on the x-axis, where zero current indicates no current flowing in the circuit. The closed channel state appears as a small negative current peaking at −0.5 (B), −0.7 (D), and −0.4 pA (F). (Bi) The small amount of open channel activity at −2.5 pA is shown in an expansion. Raw data are shown with superimposed Gaussian fits in green (WT), blue (PIEZO1$^{WT/M-R}$), and red (PIEZO1$^{M-R/M-R}$). Representative of n = 6, 5, and 4 for WT, PIEZO1$^{WT/M-R}$, and PIEZO1$^{M-R/M-R}$, respectively. (H) An exemplar recording from a PIEZO1$^{M-R/M-R}$ RBC patch with 2.5 μM GsMTx4 in the extracellular solution (n = 5).

To investigate more closely, we sought single channel data by recording from cell-attached membrane patches under voltage-clamp and applying short pressure pulses to the patch pipette to increase membrane tension. Occasionally, there was only 1 unitary current level, suggesting only 1 channel in the patch (Figure 2A,E), but in most cases, there were multiple channels (eg, Figure 2C,G). PIEZO1 channels were identified by the signature unitary current amplitude[1] (Figure 2B,D,F; supplemental Figure 11). In the WT exemplar shown, activity was evoked by the −80 and −90 mm Hg pressure pulses, but afterward, there were only infrequent openings, suggesting that this channel mostly deactivated (Figure 2A). The rarity of channel opening was seen particularly in the amplitude histogram, which indicated low frequency at −2.5 pA (channel open) relative to that at −0.5 pA (channel closed; Figure 2B). In contrast, in PIEZO1$^{WT/M-R}$ and PIEZO1$^{M-R/M-R}$ RBCs, there was identical unitary current amplitude but remarkably higher activity after termination of pressure pulses (Figure 2C-F). Histogram analysis highlighted the difference between WT and PIEZO1$^{WT/M-R}$/PIEZO1$^{M-R/M-R}$, because the frequency of open-state activity (eg, at −2.5, −2.7, and −2.4 pA) was high relative to the closed-state frequency (ie, at −0.5, −0.7, and −0.4 pA; Figure 2D,F, compare with Figure 2B). Patches containing multiple PIEZO1$^{M-R/M-R}$ channels in the same patch also showed persistent high activity (Figure 2G). Summary analysis of multichannel activity also supported the conclusion that persistent activity was greater in PIEZO1$^{WT/M-R}$/PIEZO1$^{M-R/M-R}$ (supplemental Figure 12). Unitary current events were abolished by GsMTx4 (Figure 2H).

The data suggest that RBCs provide a special environment for PIEZO1 that disables or greatly slows the rapid inactivation mechanism and confers the importance of deactivation, which is a different mechanism from that of inactivation. In future studies, it will be interesting to determine how the rapid inactivation gate is disabled or slowed in RBCs. Our work on endothelial PIEZO1 has suggested that sphingomyelinase can cause such an effect.[23] Sphingomyelinase is known to regulate RBC membrane structure[24] and adhesion of eryptotic RBCs to endothelial cells.[25] It will also be interesting to determine the molecular mechanism of deactivation in PIEZO1, its sensitivity to other DHS mutations in the RBC context, and the potential for correction by small molecules. Such studies could have multiple benefits for better understanding RBC homeostasis and DHS, and could enable better appreciation of the mechanical biology of other blood-borne cells that normally live in an environment of dynamic shear stress.

Acknowledgments

The authors thank the Blood Sciences Laboratory at Leeds General Infirmary for analysis of blood samples.

This work was supported by Wellcome Trust Investigator grant 110044/Z/15/Z and British Heart Foundation programme grant RG/17/11/33042 (D.J.B.), an Academy of Medical Sciences and Wellcome Trust Springboard Award grant SBF002\1031 (A.C.K.), and a British Heart Foundation Studentship grant FS/16/44/32356 (E.L.E.).

Authorship

Contribution: E.L.E., O.V.P., M.J.L, F.M., and L.L. performed experiments and data analyses; O.V.P. performed and analyzed the patch-clamp recordings; D.D.V. and A.C.K. generated the molecular models; M.J.L., N.E.H., and A.A. generated the PIEZO1$^{M-R/M-R}$ mouse; T.S.F. led the mouse breeding strategy; G.P. provided technical support; E.L.E., O.V.P., M.J.L., and D.J.B. designed the research; and D.J.B. raised funds to support the work and wrote the paper with the support of all authors.

Conflict-of-interest disclosure: The authors declare no competing financial interests.

ORCID profiles: E.L.E., 0000-0003-1237-7262; D.D.V., 0000-0002-7732-5095; L.L., 0000-0003-3900-786X; A.A., 0000-0002-5408-0013; A.C.K., 0000-0001-7156-9403; D.J.B., 0000-0002-7683-9422.

Correspondence: David J. Beech, Leeds Institute of Cardiovascular and Metabolic Medicine, School of Medicine, LIGHT Building, Clarendon Way, University of Leeds, Leeds LS2 9JT, United Kingdom; e-mail: d.j.beech@leeds.ac.uk; Melanie J. Ludlow, Leeds Institute of Cardiovascular and Metabolic Medicine, School of Medicine, LIGHT Building, Clarendon Way, University of Leeds, Leeds LS2 9JT, United Kingdom; e-mail m.j.ludlow@leeds.ac.uk; and Antreas C. Kalli, Leeds Institute of Cardiovascular and Metabolic Medicine, School of Medicine, LIGHT Building, Clarendon Way, University of Leeds, Leeds LS2 9JT, United Kingdom; e-mail: a.kalli@leeds.ac.uk.

Footnotes

*E.L.E. and O.V.P. contributed equally to this study.

Source data is provided online in the supplementary Data.

The online version of this article contains a data supplement.

REFERENCES

1. Coste B, Mathur J, Schmidt M, et al. Piezo1 and Piezo2 are essential components of distinct mechanically activated cation channels. *Science*. 2010;330(6000):55-60.

2. Murthy SE, Dubin AE, Patapoutian A. Piezos thrive under pressure: mechanically activated ion channels in health and disease. *Nat Rev Mol Cell Biol*. 2017;18(12):771-783.

3. Beech DJ, Kalli AC. Force Sensing by Piezo Channels in Cardiovascular Health and Disease. *Arterioscler Thromb Vasc Biol*. 2019;39(11):2228-2239.

4. Wu J, Lewis AH, Grandl J. Touch, Tension, and Transduction: The Function and Regulation of Piezo Ion Channels. *Trends Biochem Sci*. 2017;42(1):57-71.

5. Zarychanski R, Schulz VP, Houston BL, et al. Mutations in the mechanotransduction protein PIEZO1 are associated with hereditary xerocytosis. *Blood*. 2012;120(9):1908-1915.

6. Andolfo I, Alper SL, De Franceschi L, et al. Multiple clinical forms of dehydrated hereditary stomatocytosis arise from mutations in PIEZO1. *Blood*. 2013;121(19):3925-3935.

7. Albuisson J, Murthy SE, Bandell M, et al. Dehydrated hereditary stomatocytosis linked to gain-of-function mutations in mechanically activated PIEZO1 ion channels [published correction appears in *Nat Commun*. 2013;4:2440]. *Nat Commun*. 2013;4(1):1884.

8. Bae C, Gnanasambandam R, Nicolai C, Sachs F, Gottlieb PA. Xerocytosis is caused by mutations that alter the kinetics of the mechanosensitive channel PIEZO1. *Proc Natl Acad Sci USA*. 2013;110(12):E1162-E1168.

9. Glogowska E, Schneider ER, Maksimova Y, et al. Novel mechanisms of PIEZO1 dysfunction in hereditary xerocytosis. *Blood*. 2017;130(16):1845-1856.

10. Shmukler BE, Vandorpe DH, Rivera A, Auerbach M, Brugnara C, Alper SL. Dehydrated stomatocytic anemia due to the heterozygous mutation R2456H in the mechanosensitive cation channel PIEZO1: a case report. *Blood Cells Mol Dis*. 2014;52(1):53-54.

11. Del Orbe Barreto R, Arrizabalaga B, De la Hoz Rastrollo AB, et al. Hereditary xerocytosis, a misleading anemia. *Ann Hematol*. 2016;95(9):1545-1546.

12. Gnanasambandam R, Rivera A, Vandorpe DH, et al. Increased Red Cell KCNN4 Activity in Sporadic Hereditary Xerocytosis Associated With Enhanced Single Channel Pressure Sensitivity of PIEZO1 Mutant V598M. *HemaSphere*. 2018;2(5):e55.

13. Iolascon A, Andolfo I, Russo R. Advances in understanding the pathogenesis of red cell membrane disorders. *Br J Haematol*. 2019;187(1):13-24.

14. Carella M, Stewart G, Ajetunmobi JF, et al. Genomewide search for dehydrated hereditary stomatocytosis (hereditary xerocytosis): mapping of locus to chromosome 16 (16q23-qter). *Am J Hum Genet*. 1998;63(3):810-816.

15. Rotordam MG, Fermo E, Becker N, et al. A novel gain-of-function mutation of Piezo1 is functionally affirmed in red blood cells by high-throughput patch clamp. *Haematologica*. 2019;104(5):e179-e183.

16. Ma Y, Zhao Y, Cai Z, Hao X. Mutations in PIEZO2 contribute to Gordon syndrome, Marden-Walker syndrome and distal arthrogryposis: A bioinformatics analysis of mechanisms. *Exp Ther Med*. 2019;17(5):3518-3524.

17. Cahalan SM, Lukacs V, Ranade SS, Chien S, Bandell M, Patapoutian A. Piezo1 links mechanical forces to red blood cell volume [abstract]. *eLife*. 2015;4. Abstract e07370.

18. Ma S, Cahalan S, LaMonte G, et al. Common PIEZO1 Allele in African Populations Causes RBC Dehydration and Attenuates Plasmodium Infection. *Cell*. 2018;173(2):443-455 e412.

19. Rapetti-Mauss R, Picard V, Guitton C, et al. Red blood cell Gardos channel (KCNN4): the essential determinant of erythrocyte dehydration in hereditary xerocytosis. *Haematologica*. 2017;102(10):e415-e418.

20. Kaestner L, Bogdanova A, Egee S. Calcium Channels and Calcium-Regulated Channels in Human Red Blood Cells. *Adv Exp Med Biol*. 2020;1131:625-648.

21. Rode B, Shi J, Endesh N, et al. Piezo1 channels sense whole body physical activity to reset cardiovascular homeostasis and enhance performance. *Nat Commun*. 2017;8(1):350.

22. Bae C, Sachs F, Gottlieb PA. The mechanosensitive ion channel Piezo1 is inhibited by the peptide GsMTx4. *Biochemistry*. 2011;50(29):6295-6300.

23. Shi J, Hyman AJ, De Vecchis D, et al. Sphingomyelinase disables PIEZO1 channel inactivation to enable sustained response to mechanical force [published online ahead of print 4 October 2019]. *bioRxiv*. doi:10.1101/792564.

24. Abed M, Towhid ST, Mia S, et al. Sphingomyelinase-induced adhesion of eryptotic erythrocytes to endothelial cells. *Am J Physiol Cell Physiol*. 2012;303(9):C991-C999.

25. Dinkla S, Wessels K, Verdurmen WP, et al. Functional consequences of sphingomyelinase-induced changes in erythrocyte membrane structure. *Cell Death Dis*. 2012;3(10):e410.

DOI 10.1182/blood.2019004174

TO THE EDITOR:

Impact of anticoagulation prior to COVID-19 infection: a propensity score–matched cohort study

Douglas Tremblay,[1] Maaike van Gerwen,[2,3] Mathilda Alsen,[2] Santiago Thibaud,[1] Alaina Kessler,[1] Sangeetha Venugopal,[1] Iman Makki,[1] Qian Qin,[1] Sirish Dharmapuri,[1] Tomi Jun,[1] Sheena Bhalla,[1] Shana Berwick,[1] Jonathan Feld,[1] John Mascarenhas,[1] Kevin Troy,[1] Caroline Cromwell,[1] Andrew Dunn,[4] William K. Oh,[1] and Leonard Naymagon[1]

[1]Division of Hematology and Medical Oncology, Tisch Cancer Institute, [2]Department of Otolaryngology-Head and Neck Surgery, [3]Institute for Translational Epidemiology, and [4]Division of Hospital Medicine, Department of Medicine, Icahn School of Medicine at Mount Sinai, New York, NY

Coronavirus disease 2019 (COVID-19) has emerged as a global pandemic associated with a strikingly high rate of morbidity and mortality.[1,2] There is growing evidence that a pathophysiologic component of severe COVID-19 disease may be related to a provoked procoagulant state.[3-6] High rates of thromboembolic complications of COVID-19 infection have been reported,[7-11] and autopsy studies have identified evidence of macro- and microembolism in COVID-19–infected patients.[12,13] Further, perturbations of coagulation markers, most notably dramatic elevations in D-dimer levels, have been noted among COVID-19 patients and have been associated with increased mortality.[3,14]

Empiric therapeutic anticoagulation (AC) is now being used in clinical practice at many centers and will be evaluated in randomized clinical trials; however, despite the rationale for therapeutic AC, the efficacy of such an approach remains largely untested. We sought to provide evidence for or against the use of therapeutic AC among these patients. To this end, we performed a retrospective analysis of patients with confirmed COVID-19, comparing outcomes among those who were and were not receiving AC for unrelated indications at the time of COVID-19 diagnosis. Our hypothesis was that AC prior to (and during the earliest stages of) COVID-19 infection would be protective for COVID-19–related outcomes.

We retrospectively reviewed all patients with laboratory-confirmed COVID-19 diagnosed across a large New York City health system between 1 March 2020 and 1 April 2020. Confirmed COVID-19 was defined by a positive result on a reverse transcriptase polymerase chain reaction severe acute respiratory syndrome coronavirus 2 assay. Hospitalized and ambulatory patients were included in the analysis. The primary outcome was all-cause mortality. Relevant secondary outcomes included hospitalization, need for invasive mechanical ventilation, new initiation of renal replacement therapy, imaging-confirmed thrombosis, and major (World Health Organization grade ≥3) bleeding.[15] This study was approved by the Program for the Protection of Human Subjects of the Icahn School of Medicine at Mount Sinai and conducted in accordance with the Declaration of Helsinki.

To adjusted for bias due to nonrandom allocation of potential covariates among COVID-19 patients, we applied propensity score-matching methods.[16] Propensity scores were calculated using a logistic regression model, adjusting for the following